

Neuroelectromagnetic Forward Head Modeling Toolbox[☆]

Zeynep Akalin Acar*, Scott Makeig

Swartz Center for Computational Neuroscience, Institute for Neural Computation, University of California San Diego 0961, La Jolla, CA 92093-0961, United States

ARTICLE INFO

Article history:

Received 10 September 2009
Received in revised form 28 April 2010
Accepted 29 April 2010

Keyword:

MATLAB
Software
Head modeling
EEG
Boundary Element Method
BEM
Realistic
4-layer head model
MNI
Inverse problem
Source localization

ABSTRACT

This paper introduces a Neuroelectromagnetic Forward Head Modeling Toolbox (NFT) running under MATLAB (The Mathworks, Inc.) for generating realistic head models from available data (MRI and/or electrode locations) and for computing numerical solutions for the forward problem of electromagnetic source imaging. The NFT includes tools for segmenting scalp, skull, cerebrospinal fluid (CSF) and brain tissues from T1-weighted magnetic resonance (MR) images. The Boundary Element Method (BEM) is used for the numerical solution of the forward problem. After extracting segmented tissue volumes, surface BEM meshes can be generated. When a subject MR image is not available, a template head model can be warped to measured electrode locations to obtain an individualized head model. Toolbox functions may be called either from a graphic user interface compatible with EEGLAB (<http://scn.ucsd.edu/eeqlab>), or from the MATLAB command line. Function help messages and a user tutorial are included. The toolbox is freely available under the GNU Public License for noncommercial use and open source development.

© 2010 Elsevier B.V. All rights reserved.

1. Introduction

In brain electromagnetic source imaging (EMSI), the forward problem is to predict the electromagnetic fields measurable on or near to the scalp given a source distribution in the brain. For accurate source localization, the forward problem must first be solved numerically using a realistic head model. This study introduces the Neuroelectromagnetic Forward Head Modeling Toolbox (NFT), written in C++ and MATLAB. The NFT can be launched from within EEGLAB (Delorme and Makeig, 2004) or used as a standalone solver. The NFT contains tools to generate realistic BEM models from available subject data and using the METU-FP Toolkit (Akalin-Acar and Gençer, 2004) as the forward problem solver (Akalin Acar and Makeig, 2008).

Source localization and source imaging are valuable tools for investigating electrical activity in the brain. The accuracy of source localization depends largely on the head model used for source localization. Realistic head models employing the Boundary Element Method (BEM) or the Finite Element Method (FEM) allow more accurate calculation of the electrical and magnetic fields

compared to simple spherical head models. High quality and high performance BEM and FEM forward problem solvers are available to the scientific community (Akalin-Acar and Gençer, 2004; Gençer and Acar, 2004; Wolters et al., 2002). However, most researchers use either spherical head models or numerical methods employing relatively simple, template-based head models. The main reason for this is the difficulty of creating high quality, realistic, subject-specific head models. The goal of the NFT is to assist the user in generating such head models using any and all available information about the subject and recording session, and to provide a convenient interface for using the resulting models in functional BEM-based source imaging.

Source localization accuracy and performance of analytical head models have been investigated by many researchers. Henderson and Butler (1975) tested a saline filled conductor and a spherical head model, reporting a mean 1-cm localization error. Cohen et al. (1990) used sources implanted within a human brain. Using spherical head models, the average localization error was 8 mm for MEG and 10 mm for EEG. Weinberg et al. (1986) used a human skull with implanted sources and obtained a mean 3.5-mm localization error using a head model that used 25 spheres to model the skull. Zhang et al. showed that large errors may occur when estimating the parameters of two simultaneously active dipoles when the shell model is misspecified (Zhang and Jewett, 1993; Zhang et al., 1994). These results suggest that analytical head models are not sufficient for accurate source localization.

[☆] This work is supported by NIH (NS047293-04), NSF (0613595), and a gift from The Swartz Foundation (Old Field, NY).

* Corresponding author. Tel.: +1 858 822 7536; fax: +1 858 822 7556.
E-mail addresses: zeynep@scn.ucsd.edu (Z.A. Acar), scott@scn.ucsd.edu (S. Makeig).

The desire for more accuracy has led to the use of realistic numerical head models. Roth et al. (1993), Crouzeix et al. (1999), and Cuffin (1996) investigated dipole localization accuracy using spherical and realistic meshes in a 3-layer BEM model. They found that dipole localization improves by 1–2 cm when realistic head models are used. Ramon et al. (2004) examined the effects of soft skull bone, cerebrospinal fluid (CSF) and gray matter on distribution of scalp potentials using the finite element method (FEM). They observed that the scalp potentials were significantly affected by these tissues. Thus, the accuracy of source localization can further be improved when more realistic head models are used in forward problem solutions.

One of the difficulties in creating realistic head models is to create the head mesh that provides the geometry and conductivity information to the numerical solver. This is usually done by segmenting 3-D structural magnetic resonance (MR) and/or computed tomography (CT) images. Some tools available for extracting the brain and skull surfaces from MRI images include a Brain Extraction Tool (BET) by Smith (2002), ANATOMIC by Heinonen et al. (1998), and BBrain Image ANalysis (BRIAN) by Kruggel and Lohmann (1996). FreeSurfer (<http://surfer.nmr.mgh.harvard.edu/>) provides tools to extract a high quality brain surface and to register it with the Talairach atlas (Talairach and Tournoux, 1998). Commercial software packages such as ANALYZE and CURRY can also be used to extract skull, scalp and brain surfaces from MR images. The segmentation tools provided by these software packages are not completely automated and require user input to some degree.

Various toolkits are available for segmentation and source localization. BrainVisa/Anatomist is an open source toolkit written in Python for extracting cortical surfaces and performing EEG/MEG source localization (Riviere et al., 2003). BrainSuite is a freely available Windows application for extracting scalp, skull, CSF and brain tissues (Shattuck and Leahy, 2002). FreeSurfer, which provides advanced MRI segmentation, and surface extraction is also open source and freely available for research purposes. MNE is a free toolkit linked to FreeSurfer for EEG/MEG analysis. It uses a combination of C and MATLAB, but source code is not available (<http://www.nmr.mgh.harvard.edu/martinos/userInfo/data/sofMNE.php>).

The lack of unified and freely available segmentation and mesh generation tools has inhibited the use of high-quality realistic head models in brain electrophysiology research. Most researchers continue to use either spherical head models, a fixed template head mesh such as the Montreal Neurological Institute's (MNI) template head model, or low-quality realistic models. Other factors preventing the widespread use of subject-specific realistic head models include computational requirements and the unavailability of MR head images for many subjects.

NFT began as an effort to integrate existing realistic forward problem solvers, segmentation and mesh generation tools we have developed in previous research. It runs under MATLAB and to save time uses freely available C++ executables to generate BEM matrices and for some steps of mesh generation. NFT MATLAB was developed under MATLAB 7.3 and requires the MATLAB image processing toolbox. The state-of-the-art BEM solver was developed in C++ and released as the METU-FP toolkit (Akalin-Acar and Gençer, 2004). While developing the toolbox, some of the functionality of the forward problem solution is ported to MATLAB for better integration, but, re-implementing the BEM matrix generation would have required a lot of extra development and testing and would have increased the memory requirements and computing time. BEM mesh generation also began as native code (C or C++). Open source tools and libraries such as ASC and Qslim are used for triangulation and coarsening respectively. While MATLAB toolboxes exist that allow similar functionality, using existing open source tools allowed us to reduce development and testing considerably. Using MATLAB as the integration platform made it easier to develop

the graphical user interface (GUI) and to interface to the EEGLAB environment and to native code tools. This made it possible to focus on providing a consistent user interface to the underlying tools, including providing default parameters that result in good quality head models.

The NFT is released under an open source license, allowing researchers to contribute to and improve on this work for the benefit of the neuroscience community. By bringing together advanced head modeling and forward problem solution methods and implementations within an easy to use toolbox, the NFT complements the widely used EEGLAB environment, an open source toolkit under continued development (Delorme and Makeig, 2004). Combined, NFT and EEGLAB form a freely available EEG (and in future, MEG) source imaging solution and an attractive environment for introducing advanced inverse source localization methods into research laboratories and courses.

NFT implements the major aspects of realistic head modeling and forward problem solution from available subject information:

1. *Segmentation of T1-weighted MR images*: The preferred method of generating a realistic head model is to use a 3-D whole-head structural MR image of the subject's head. The toolbox can generate a segmentation of scalp, skull, CSF and brain tissues from a T1-weighted image.
2. *High-quality BEM meshes*: The accuracy of the BEM solution depends on the quality of the underlying mesh that models tissue conductance-change boundaries. To avoid numerical instabilities, the mesh must be topologically correct with no self-intersections. It should represent the surface using high-quality elements while keeping the number of elements as small as possible. The NFT can create high-quality linear surface BEM meshes from the head segmentation.
3. *Warping a template head model*: When a whole-head structural MR image of the subject is not available, a semi-realistic head model can be generated by warping a standard template BEM mesh to the digitized electrode coordinates (instead of vice versa).
4. *Registration of electrode positions with the BEM mesh*: The digitized electrode locations and the BEM mesh must be aligned to compute accurate forward problem solutions and lead field matrices.
5. *Accurate high-performance forward problem solution*: The NFT uses a high-performance BEM implementation from the open source METU-FP Toolkit (Akalin-Acar and Gençer, 2004) for bioelectromagnetic field computations.

The NFT has two major parts; generation of realistic head models and numerical solution of the forward problem. Toolbox functions are detailed in Section 2. Section 3 describes the toolbox components, together with some screenshots from the GUI. In Section 4, examples of NFT head models are shown and the accuracy and efficiency of BEM-based equivalent dipole localization is estimated.

2. Toolbox functionality

This section describes forward problem solutions, image segmentation, mesh generation, template warping, and co-registration of the electrode locations.

2.1. Boundary Element Method

The Boundary Element Method (BEM) is a numerical computational technique for solving partial differential equations. In electromagnetic source imaging (EMSI) of brain activity, BEM may be used to solve the forward problem using realistic head models. When using BEM for head modeling, the head is assumed to be com-

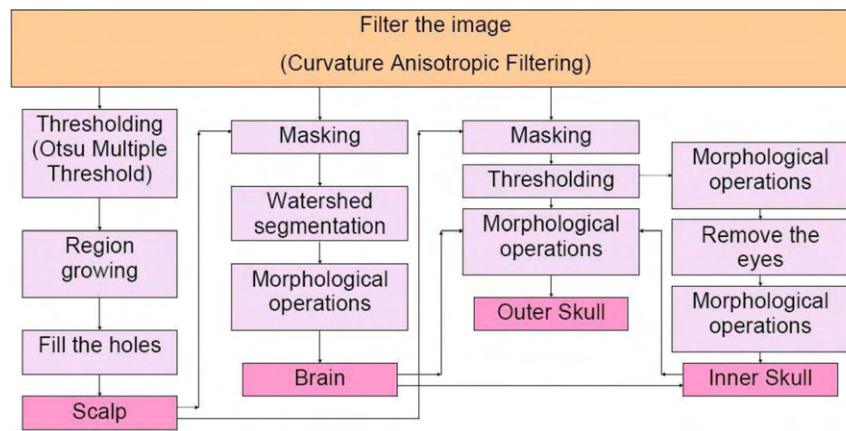


Fig. 1. The segmentation algorithm used in NFT. Scalp, brain, outer skull, and inner skull are segmented using filtering, thresholding, region growing, morphologic operations, and watershed segmentation.

posed of uniform conductivity regions (i.e., scalp, skull, brain, etc.) whose tissue boundaries may be represented by triangular surface elements.

The properties of the BEM implementation may be summarized as follows:

1. To eliminate possible singularities in the BEM matrix, the method of matrix deflation (Lynn and Timplake, 1968) is employed.
2. The Isolated Problem Approach (IPA) is used to overcome numerical errors caused by large conductivity differences near the skull layer. The IPA used in this implementation of BEM is generalized to allow layers within the modified boundary which is the inner skull. It has been shown that this implementation of IPA corrects the electric field by 11–15% (RDM) for tangential dipoles, and 11–217% for radial dipoles in a 4-layer spherical head model (Gençer and Akalın-Acar, 2005).
3. A recursive integration technique is employed to increase the accuracy of the BEM implementation. In recursive integration, the surface elements are divided into sub-elements and numerical integration is performed on each sub-element. This process is repeated recursively until a subdivision criterion is met. Since the potential field is calculated at the original nodes, the size of the BEM matrix equation remains the same, but the accuracy of the computed surface integral is improved.
4. The BEM implementation allows the use of quadratic surface elements in realistic head models for increased accuracy with a smaller number of elements.
5. Intersecting tissue boundaries are supported by allowing the BEM mesh to have more than two elements sharing a single edge. This allows modeling of complex tissues such as eyes. Currently, the toolbox does not support generating intersecting meshes, but can use them if they are generated externally. The validation of intersecting surfaces is given in (Akalın-Acar and Gençer, 2004) by comparing BEM solutions with FEM solutions using a 3-layer head model with a disk-shaped inhomogeneity intersecting the skull layer. The electric field differences for different dipole positions and varying conductivity of the inhomogeneity between BEM and FEM solutions were smaller than 1%.
6. To decrease computation time, transfer matrices are computed that relate source projections to field strengths at given sensor locations. By pre-computing transfer matrices, forward solutions of electric and magnetic field problems are reduced to simple matrix–vector multiplications.

More details of the BEM formulation and its accuracy using simple spherical head models can be found in Gençer and Tanzer

(1999), Akalın-Acar and Gençer (2004) and Gençer and Akalın-Acar (2005).

2.2. Segmentation

When tomographic images of the subject's head are available, it is possible to create a realistic model of the head tissue boundaries. Since T1-weighted MR images are now commonly acquired for structural imaging, the toolbox makes use of T1-weighted images, when available, to generate a 4-layer head model consisting of scalp, skull, CSF, and brain surfaces. The segmentation algorithm used in this study is shown in Fig. 1.

The segmentation procedure starts with anisotropic filtering of the 3-D head image to enhance image quality. This smooths the image while preserving gradient (boundary) information (Ibanez et al., 2005). Filtering is followed by scalp segmentation. The threshold for the scalp surface boundary is found by Otsu thresholding (Nobuyuki, 1979). After thresholding the 3-D image, the resulting binary image is morphologically closed. The toolbox then applies 3-D region growing to eliminate any image noise outside the scalp. Finally, any holes in the scalp are filled by applying the 'filling' morphological operation in the sagittal, coronal and axial directions. For anisotropic filtering and Otsu thresholding, the MATITK MATLAB interface to the ITK image processing toolkit is used (Chu and Hamarneh, 2005). The morphological operations are performed using functions from MATLAB's image processing toolbox.

For brain segmentation, a watershed segmentation algorithm from the ITK toolkit is used (Ibanez et al., 2005). After masking the filtered MR image with segmented binary scalp image, an initial brain segmentation is performed using watershed segmentation. This initial brain volume also includes skull marrow where the skull is thin in the MR image. To eliminate the bone marrow, thresholding, morphological erosion and dilation, and region growing operations are applied. In some cases, the watershed segmentation includes tissues below the cerebellum such as the brain stem and inferior scalp tissues. To prevent this, the lower boundary of watershed segmentation is limited by a user-supplied indication of the lowest point of the cerebellum.

While soft tissues are easy to identify from T1-weighted MR images, it is difficult to distinguish skull from CSF and other head cavities (sinuses). Therefore, skull and cerebrospinal fluid (CSF) (inner skull) boundaries are deduced from segmented masks for the scalp and the brain.

An initial segmentation for outer skull is performed by thresholding the filtered MR image with the scalp mask. For final skull segmentation the segmented, eroded, and closed inner skull volume is used. For some subjects, the eyes remain connected to the

skull. To prevent this, the user selects a point in each eye from an axial view in which the eyes are seen clearly. The eyes are extracted by region growing from the user-indicated points.

The CSF boundary is obtained from the eroded skull and dilated brain boundaries. At the end of segmentation, the skull and scalp surfaces are improved to avoid thin regions in the skull.

2.3. Mesh generation

To solve the forward problem, the geometrical information obtained by image segmentation should be converted into a numerical form (i.e., as a set of meshes). To generate the BEM surface meshes, an improved version of the mesh generation algorithm described by Akalın-Acar and Gençer (2004) is used. The steps for generating surface meshes from segmented 3-D volume images are described below.

The first step in mesh generation is the triangulation of the segmented image. For this purpose, an implementation of the adaptive skeleton climbing (ASC) algorithm is used that is freely available for academic, research and internal business purposes (Poston et al., 1998). For each tissue, the volume is converted to a raw format compatible with the ASC application. It is then triangulated using ASC which places one or more triangles in each boundary voxel. This results in a very fine mesh representing the tissue surface. This mesh needs further processing and coarsening, however, before it can be used as a BEM mesh.

The triangulated surface is then smoothed using a surface signal low-pass filter algorithm (Taubin, 1995). This smoothing helps suppress high frequencies caused by noise and slice effects in the MR image. During the smoothing process, the vertices of the triangulated surface are moved but the connectivity of the faces remains unchanged.

The number of mesh triangles is reduced using a coarsening algorithm based on iterative edge contraction and quadric error metrics (Heckbert and Garland, 1999). For this purpose, the QSLim tool is used, an open source tool available under the GPL license (Garland and Shaffer, 2002). At every coarsening step, the neighbor nodes with lowest errors are connected and a coarser mesh is obtained.

The resulting mesh may still contain some undesirable topological artifacts such as disconnected or multiply-connected element edges and singular nodes. These artifacts are corrected to create a single manifold surface that represents the given surface boundary (Guziec et al., 2001). To summarize, multiple iterations of the following steps are performed to obtain a topologically correct, high quality mesh:

- Any isolated vertices (those with no elements attached) are identified and removed.
- Edges with more than two elements are marked and corrected (Guziec et al., 2001).
- For each edge, neighboring elements are checked; the edge is flipped, if possible, to improve the aspect ratio of the elements.
- Very small face elements are identified and removed.
- Elements with poor aspect ratios (elements where the ratio of the shortest edge to longest edge is smaller than 0.3) are identified and removed.
- Isolated groups of elements are removed.

As previously shown, the accuracy of BEM inverse solutions depend on the eccentricity of the dipoles. As the dipoles approach the brain surface, forward problem solution accuracy decreases; when the meshes are refined, solutions become more accurate (Roth et al., 1993; Akalın-Acar and Gençer, 2004). A theoretical reasoning for this fact was given in Drechsler et al. (2009) and Wolters et al. (2007). Another type of inaccuracy occurs when two mesh lay-

ers are too close to each other. If the distance between two meshes is less than the edge length of the neighboring elements, then the accuracy of the numerical solutions decreases. NFT handles this by performing local mesh refinement in regions where neighboring meshes are close to each other.

The aim of local mesh refinement is to make sure that the distance between meshes is not too small compared to edge length, of the neighboring elements. For this purpose, mesh elements with relatively long edges are refined when their edge length is larger than the local distance of two neighboring meshes. For each surface, edges that are close to the outer neighboring surface are detected, and elements belonging to that edge are refined. This is repeated until there are no large edges close to the neighboring surface. This procedure is repeated for all surfaces beginning from the innermost layer. The local mesh refinement (LMR) ratio used for this purpose is computed as: $LMR_{(node,mesh)} = (\text{mean edge length})/(\text{mesh distance})$, where the mean edge length of the node is calculated by averaging the lengths of all the edges connected to that node, and mesh distance is the shortest distance from the node to the neighboring mesh.

2.4. Registration of electrode locations and scalp surface

After creating the head model from the MR image, electrode locations must be mapped onto the scalp mesh. It is assumed that the coordinate systems of the digitizer and the MRI can be mapped through a rigid-body transform (rotation and translation). For registering the electrode locations to the head model, the rigid-body transform parameters that can best match the scalp and the electrodes are computed. For this purpose, six parameters of rotation and translation are calculated so as to minimize the total squared distance between the scalp mesh and the electrode positions using non-linear optimization (Akalın-Acar and Gençer, 2004).

2.5. Warping

When the MR image of the subject head is not available, a frequently used approach to source localization is to map the recorded 3-D electrode locations to a mean subject template head mesh. An alternative approach suggested by Darvas et al. (2006) is to warp a template mesh to fit the observed sensor locations. NFT implements this approach to generate subject-adapted head models when MR images are not available. This results in more realistic head models compared to mapping electrodes to a template mesh.

Scalp surface warping parameters are computed based on three fiducial points: the nasion and left and right preauricular points (Fig. 2). The preauricular points are defined as the bony indentation in front of the ears. The nasion is the bridge of the nose at the forehead. From these three points, the vertex of the scalp is computed in both the template model and the subject head surface implied by the recorded electrode locations. Using these four points, the sensor locations and head model are brought into same coordinate system.

After this initial co-registration, 19 landmarks are located on both the head model and sensors, as described in Darvas et al. (2006). These landmarks are used to find the best-fitting warping parameters using a non-rigid thin plate spline method (Bookstein, 1999). All the surfaces and the source space are warped using the same warping parameters. Reverse warping parameters that warp the sensor coordinates to the template mesh are also computed. These parameters can be used to map source localization results to the template head.

3. NFT components

After installing and configuring the toolbox, one may start it by typing, on the MATLAB commandline:

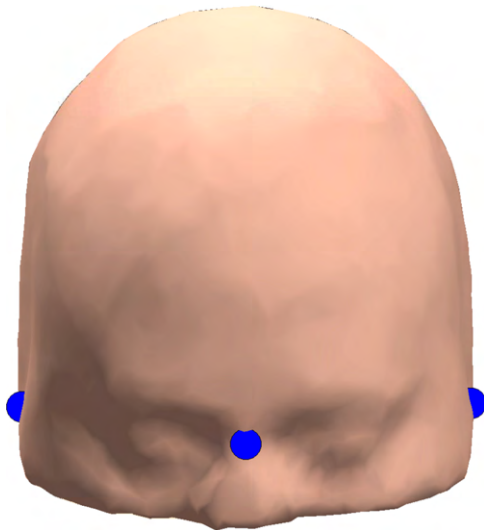


Fig. 2. The nasion and left and right preauricular points shown on an MNI head model.

» Neuroelectromagnetic_Forward_Modeling_Toolbox
or, if preferred,
» NFT

The main NFT window appears as shown in Fig. 3. This window is divided into three panels. The top panel is used to select the working folder and to name the subject and session. The lower panel is the head modeling panel. The lowest panel in the main NFT menu initiates forward model generation, opening the forward model generation interface used to compute the BEM coefficient

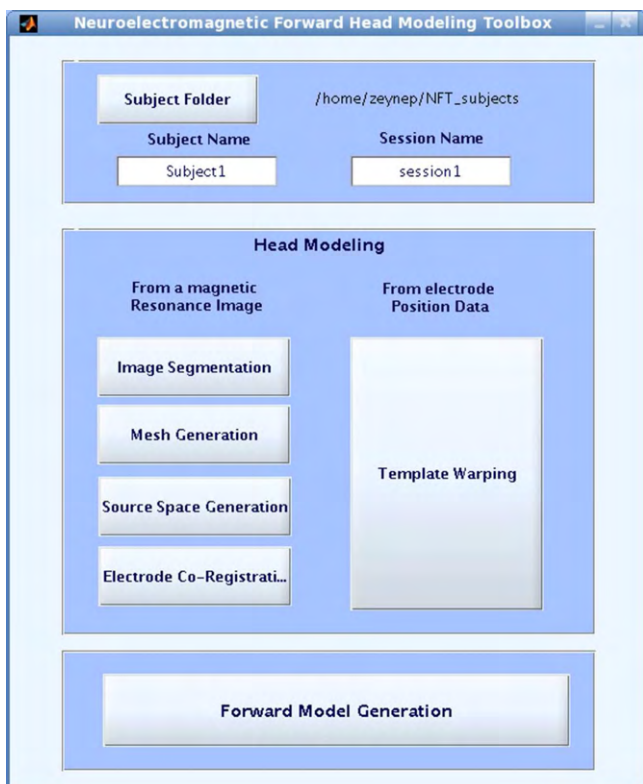


Fig. 3. The NFT main user interface. This window is divided into three panels. The top panel is used to select the working folder and to name the subject and session. The lower panel is the head modeling panel. The lowest panel in the main menu of NFT cues forward model generation.

matrix, create the transfer matrices for each sensor, and generate lead field matrices for a given source distribution.

In the following sub-sections, NFT module components are introduced. Inputs and outputs of each module are explained and their user interfaces are illustrated.

3.1. Head modeling: segmentation

The input to the segmentation module is a T1-weighted MR image. When the image is loaded, sagittal, axial, and coronal slices are shown for an indicated voxel. It is easy to change the slices displayed by using the scroll bars or clicking on the images (Fig. 4). The *Display image* panel allows the user to select which image volume to display. The available choices are the MR volume, the filtered volume, or the image volume in various stages of segmentation.

The segmentation algorithm does not perform well for volumes effected by inhomogeneity artifacts. The “Check inhomogeneity” button checks whether the current image volume needs inhomogeneity correction or not. The adjacent checkbox “Swap L|R” can be used to exchange left and right when needed.

Segmentation steps are performed in this order:

1. Anisotropic filtering. (User inputs: filter parameters.)
2. Scalp segmentation.
3. Brain segmentation. (User input: A seed point for brain segmentation; the lowest point of the cerebellum.)
4. Outer skull segmentation. (User input: A seed point near the center of either eye.)
5. Inner skull segmentation.

The segmentation module outputs filtered MR images and scalp, skull, CSF, and brain masks. It is possible to save the results of any stage of segmentation in MATLAB data format. The filtered MR images are saved in MATLAB double precision; the masks are saved as a MATLAB structure.

Fig. 5 shows segmentation results for scalp, skull, CSF, and brain for four subjects whose MR head images were acquired using a 3-T GE scanner.

3.2. Head modeling: mesh generation

The second step in realistic head modeling is mesh generation. The NFT mesh generation module uses the results of the segmentation and outputs either 3-layer or 4-layer BEM head meshes. A 3-layer mesh includes scalp, outer skull, and CSF surfaces. The CSF and the brain are considered a single region. A 4-layer mesh models scalp, skull, CSF, and brain by including an additional inner skull surface separating the CSF from the brain. It is also possible to apply local mesh refinement to locally refine the meshes where one surface comes close to a neighbouring surface.

The *mesh generation* interface is shown in Fig. 6. The generated mesh file can be used directly by the BEM solver.

Fig. 7 shows the meshes generated for the volumes shown in Fig. 5.

3.3. Source space generation

A source space is a set of dipole sources placed within the brain volume. It is used to generate the lead field matrix (LFM) that maps the amplitudes of possible dipolar sources to electrode potentials. An LFM using a regular grid source space can be used for single-dipole parametric inverse problem solution to give a coarse estimate of source location.

The NFT contains an option to generate a simple dipolar source space consisting of a regular 3-D voxel grid. The grid is generated by placing three orthogonal dipoles at each grid location inside the

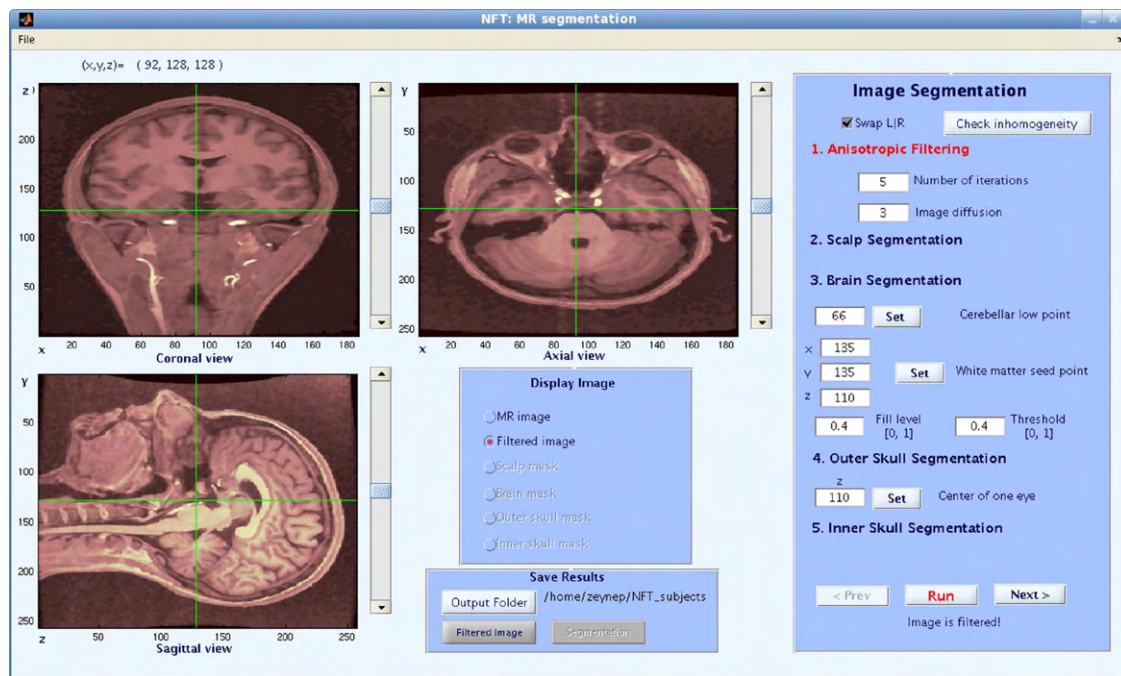


Fig. 4. The NFT head tissue segmentation interface. When a T1-weighted MR image is loaded, anisotropic filtering, scalp, brain, outer skull, and inner skull segmentation are performed.

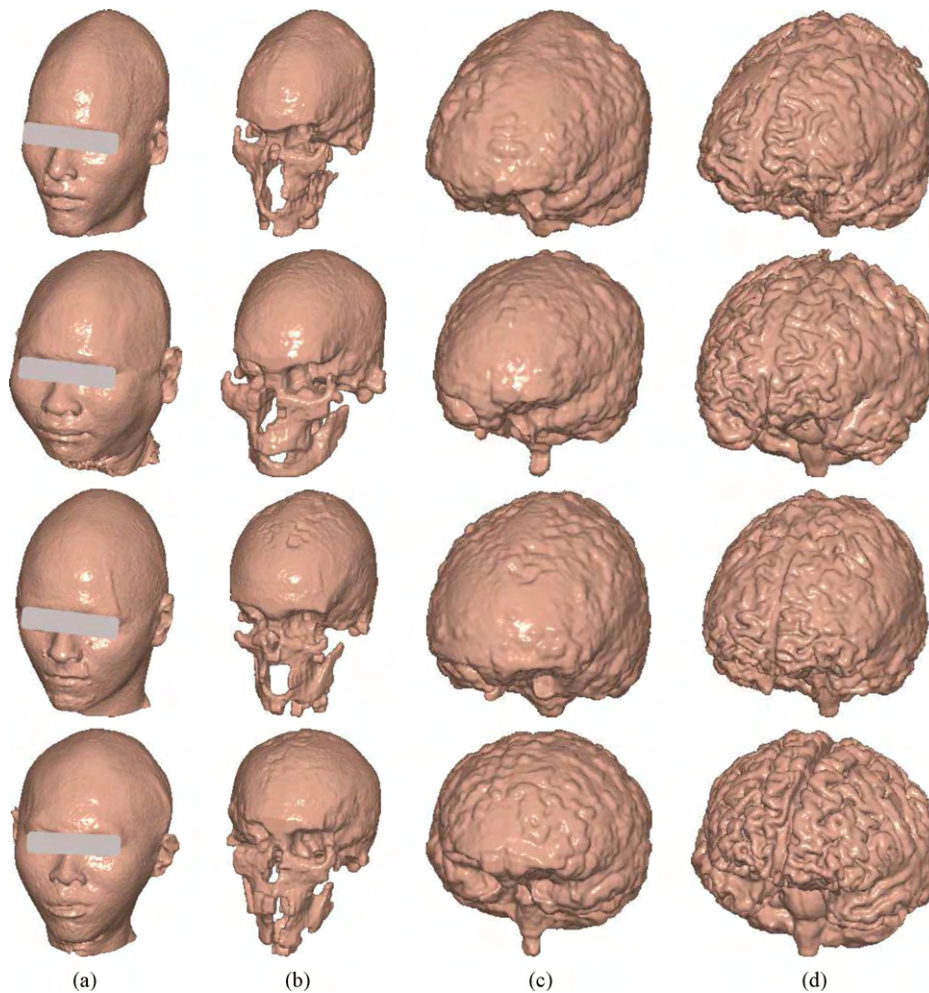


Fig. 5. Segmentation results showing (a) scalp, (b) skull, (c) CSF and (d) brain volumes computed from four subject MR head images acquired using a 3-T GE scanner.

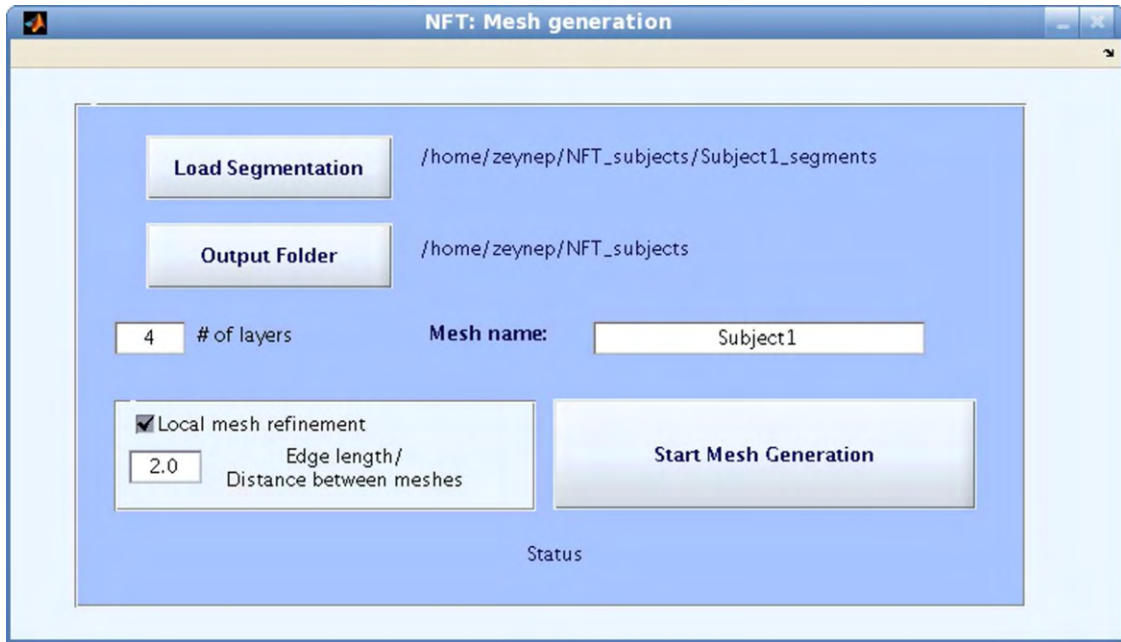


Fig. 6. The NFT mesh generation user interface. The mesh generation module uses the results of the segmentation and outputs either 3-layer or 4-layer BEM head meshes.

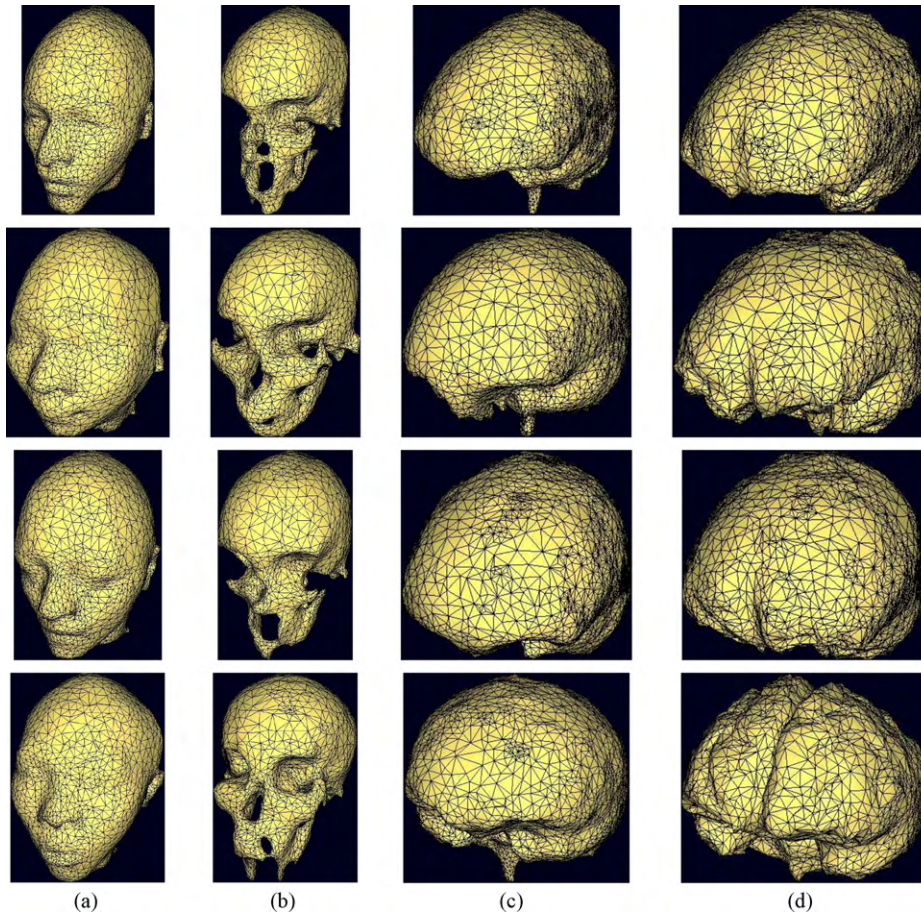


Fig. 7. BEM models of the scalp, skull, CSF and the brain for four subjects: (a) scalp mesh, (b) skull mesh, (c) CSF mesh, (d) brain mesh generated for the volumes shown in Fig. 5.

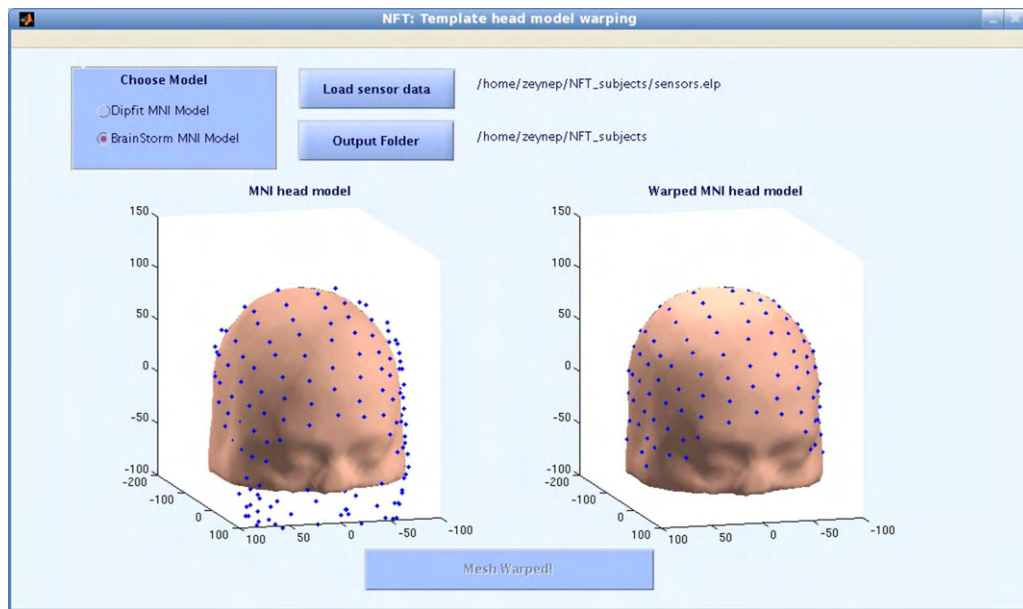


Fig. 8. The NFT user interface for warping a template head model to measured 3-D electrode locations.

brain volume. User inputs are the spacing between the dipole elements and the minimum distance of a dipole element to the brain mesh. The grid spacing determines the minimum distance between two dipoles.

3.4. Co-registration of electrode locations

The BEM mesh is generated from the 3-D MR volume and uses the same coordinate system as the MR volume. When working with EEG recordings, the electrode coordinates measured by a digitizer must be mapped to the mesh coordinates. This step is called co-registration of electrode locations to the mesh volume. The input to the electrode co-registration module is the set of electrode locations. The subject scalp mesh is loaded automatically and the electrodes are co-registered to the scalp mesh. The co-registration is accomplished in two steps. First the user manually roughly co-registers the sensors. The second, automated step finds the translation and rotation parameters that minimize the total squared distance between the sensors and the model scalp surface.

3.5. Head modeling using template warping

When the MR image of the subject head is not available, the toolbox can generate a subject-adapted template head model. The template head model is warped to the electrode locations (rather than warping the electrode positions to the template head model). The warping is based on three fiducials: the nasion and left and right preauricular points. The inputs of the warping module are these fiducials and the electrode locations (obtained from a 3-D position digitizer). The outputs are the warped mesh,

the warped source space, indices of the electrodes on the mesh, fitted electrode locations, and the warping parameters. The warping parameters may be used to warp the localized sources back to the template model. The template head model included in the toolbox is based on the MNI averaged MR image available at <http://www.bic.mni.mcgill.ca/software/>. It is possible to use another head model as a template head model by replacing the template mesh files as long as corresponding fiducials and landmarks are also specified. Note that the number of warped electrodes may be lower, since the MNI head is not a complete whole-head model and some electrodes on the neck might lie below the template mesh. Fig. 8 shows the user interface for the warping module, and in Fig. 9, a warping result is shown in different views.

3.6. Forward problem solutions: BEM

The forward problem solution module is written mainly in MATLAB and includes a set of functions to read the mesh, generate the BEM matrices, register the electrodes to the BEM mesh, and compute the forward problem solution and lead field matrices. These functions can also be accessed using the user interface. The BEM user interface is shown in Fig. 10.

The binary BEM solver that computes the BEM matrices is an executable program written in C++ that is launched from MATLAB with parameters necessary to compute and save the BEM matrices. The solver is called transparently by MATLAB and need not be called explicitly by the user.

The user interface for the forward problem module uses three MATLAB data structures to store the state of forward problem com-

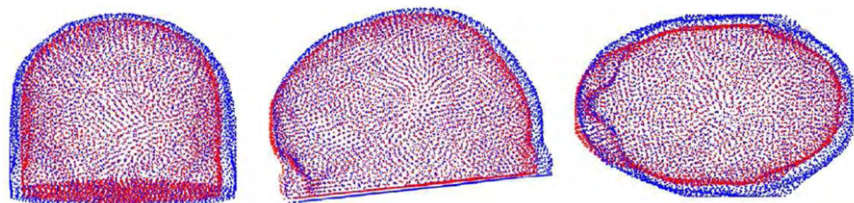


Fig. 9. Three views of the nodes of the template mesh (blue) and the warped mesh (red). The warped mesh fits the electrode locations.

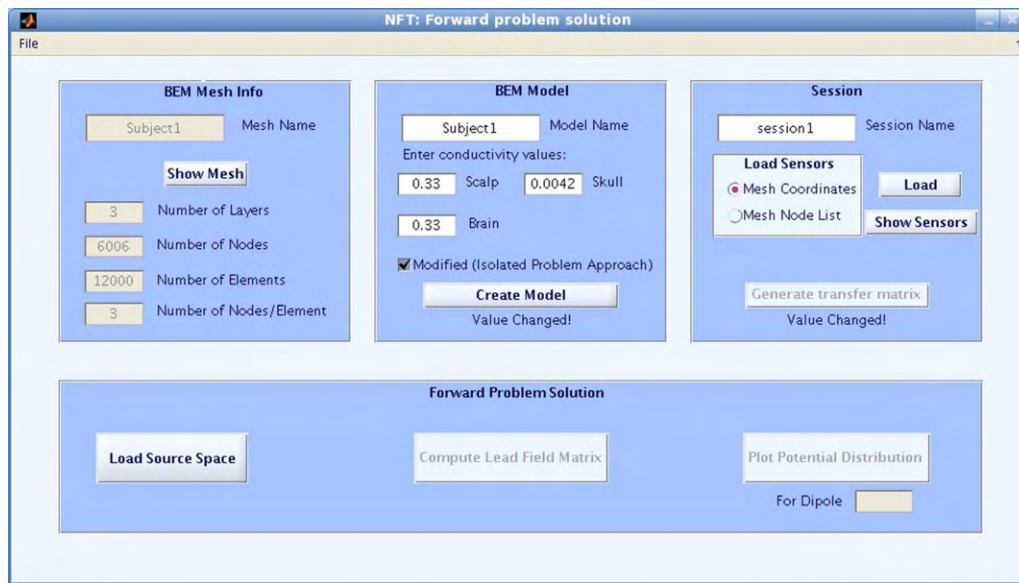


Fig. 10. The NFT BEM construction user interface has four panels: (Upper panels) Load a mesh, load or generate BEM meshes, load or generate transfer matrices. (Lower panel) Predict scalp potentials produced by given dipole(s).

putations:

- The *mesh structure*: stores the mesh information, i.e., the geometry of the head.
- The *model structure*: holds the mesh coefficients, solver (i.e., IPA) parameters, and tissue conductivities.
- The *session structure*: contains the model structure and electrode coordinates on the mesh.

A BEM forward problem solution proceeds through the following steps:

1. Compute the BEM matrices for the given head model.
2. Compute the transfer matrix for the given set of electrode locations.
3. Obtain the electrode potentials generated by activity of each source dipole.

The default conductivity values for scalp, skull, and brain are set to 0.33, 0.0042, and 0.33 S/m, respectively (Geddes and Baker, 1967). In Baumann et al. (1997), CSF conductivity at body temperature was found to be 1.79 S/m, here used by default. The toolbox allows the user to change these values using the forward problem solution GUI. In this study we used the default values.

The toolbox can also make use of the MATLAB Parallel Processing toolbox (if installed) to distribute the computation of the transfer and lead-field matrices to multiple processors. To do this, before running NFT, the user must simply enter

```
>> matlabpool(n) % n: the number of compute nodes available
```

In parallel mode, wait bars do not appear while computing the transfer and lead-field matrices.

4. Results

This section presents statistics on the runtime performance of the toolbox and the effect of local mesh refinement, and gives an example of source localizations obtained using different head models.

4.1. Computational complexity

The computational cost of using a realistic head model is related to the size of the BEM matrices, which depend on the number of nodes in the meshes. The aim of this section is to indicate how long different stages of the head modeling and forward problem solution require on current (2009) computers.

In this section, a 4-layer realistic model generated from an MR head image is used. The mesh had 16,016 nodes, and 32,024 faces in all. Local mesh refinement used an LMR ratio of 2. The scalp, skull, CSF, and brain surfaces had 6944, 7084, 9298, and 8698 elements, respectively.

Table 1 shows computation times for realistic head modeling and forward model generation of a head model from an MR image. These computations used a single 2.4-GHz 64-bit Opteron processor.

Table 2 shows the computation times for forward model generation when the head model was obtained by warping a template head model. Warping a template head model and source space generation required only a few seconds, so these are not given in the tables.

The memory used for matrix computations is slightly larger than the total size of the BEM matrices. The in-memory size of the BEM

Table 1
Computational complexity for the realistic model.

Segmentation	25 min
Mesh generation	38 min
Co-registration	25 min
BEM matrix generation (16,016 nodes)	120 min
Transfer matrix calculation (141 sensors)	192 min
Lead field matrix calculation (6075 dipoles)	60 min
Total	735 min (7.25 h)

Table 2
Computational complexity for the warped model.

Generation of BEM matrices (6006 nodes)	19 min
Calculation of the transfer matrix (135 sensors)	15 min
Calculation of the lead field matrix (10,131 dipoles)	30 min
Total	64 min (1.1 h)

Table 3

Relative difference measures (%RDMs and RDM*s) for various tangential (x -directed) dipoles located on the z axis ($z = 1 - 6$ cm) in a 4-layer spherical head model. The results are presented for solutions with and without the use of IPA.

Distance (cm)	With IPA		Without IPA	
	%RDM	RDM*	%RDM	RDM*
1.0	0.30	0.0006	28.44	0.0105
1.5	0.31	0.0009	28.53	0.0109
2.0	0.31	0.0012	28.65	0.0112
2.5	0.31	0.0015	28.79	0.0116
3.0	0.32	0.0018	28.95	0.0120
3.5	0.32	0.0022	29.12	0.0124
4.0	0.33	0.0026	29.34	0.0139
4.5	0.35	0.0031	29.81	0.0198
5.0	0.39	0.0037	30.91	0.0354
5.5	0.44	0.0044	31.10	0.0503
6.0	1.42	0.0118	32.45	0.1366

matrix is $N \times N \times 8$ bytes, where N is the number of nodes and each entry uses 8 bytes for double precision floating point. If IPA is applied, then two additional matrices are also calculated and stored. These two matrices consume $N_1 \times N \times 8$, and $N_2 \times N_2 \times 8$ bytes respectively, where N_1 is the number of nodes of the skull layer and N_2 is the number of nodes in the inner layers (CSF and brain if a 4-layer model is used). Similar realistic subject-specific head models generated by NFT using IPA would require approximately 4.8 GB of memory.

The transfer matrix computation and lead-field matrix generation steps may be executed on multiple processors if the MATLAB Parallel Processing Toolbox is available. We have measured a 2.6 \times speed-up by generating the transfer matrix on a quad-core instead of a single core processor.

4.2. Accuracy of the BEM implementation

To assess the accuracy of the BEM solutions, we performed an error analysis, comparing analytical solutions with numerical solutions obtained using a 4-layer spherical BEM head model. The four layers representing brain, CSF, skull, and the scalp had conductivities 0.33, 1.79, 0.0042, and 0.33 S/m, respectively. The radii of the model spheres were 61, 65, 71, and 75 mm as recommended in Meijs et al. (1989). The analytical solutions provided by Kavanagh et al. (1978) were compared with the NFT numerical solutions using the RDM and RDM* metrics (Meijs et al., 1989).

A similar error analysis was performed in Gençer and Akalin-Acar (2005) for the same BEM implementation. We used the same spherical quadratic BEM mesh which has 512 elements and 1026 nodes per layer. The only difference in the head model is the conductivity of the CSF. The previous study used 1.0 S/m for CSF conductivity. This study used 1.79 S/m to match the value reported by Baumann et al. (1997).

Percentage RDM and RDM* values for various tangential (x directed) dipoles along z axis are given in Table 3. The numerical solutions were computed twice, once with IPA and once without IPA. Application of IPA improved the solutions significantly. Compared to the earlier study of Gençer and Akalin-Acar (2005), the RDM and RDM* values are very close when IPA was applied, while for the solutions derived without using IPA the RDM values almost doubled because of the higher conductivity difference at the skull boundary used in this study. The use of IPA eliminates this error.

Table 4 gives the same information for radial (z directed) dipoles. The errors were higher for radial dipoles compared with tangential dipoles as the dipole was closer to the surface. The accuracy of the numerical solutions depends on how well the mesh elements can match changes in the field. For tangential dipoles, the change in the field is distributed over many elements. For radial

Table 4

Relative difference measures (%RDMs and RDM*s) for various radial (z -directed) dipoles located on the z axis ($z = 1 - 6$ cm) in a 4-layer spherical head model. The results are presented for solutions with and without the use of IPA.

Distance (cm)	With IPA		Without IPA	
	%RDM	RDM*	%RDM	RDM*
1.0	0.31	0.0009	28.21	0.0103
1.5	0.34	0.0019	28.02	0.0104
2.0	0.49	0.0040	27.74	0.0112
2.5	0.78	0.0073	27.36	0.0136
3.0	1.23	0.0120	26.88	0.0184
3.5	1.83	0.0181	26.31	0.0259
4.0	2.56	0.0255	25.80	0.0364
4.5	3.41	0.0339	25.51	0.0505
5.0	4.33	0.0431	24.17	0.0743
5.5	5.45	0.0512	26.08	0.2536
6.0	13.61	0.0338	277.76	1.9164

dipoles, however, the rapid changes in the field need to be handled by increasingly smaller elements as the dipole position is closer to the surface. Using smaller elements helps increase this accuracy, as does using higher order elements.

Note that, the dipole at $z = 6$ cm is only 1 mm away from the brain layer which accounts for the increased error for this dipole.

4.3. Source localization comparisons

This section presents source localization results using various head models. First, simulation studies are presented that compare single dipole source localization differences between 3-layer and 4-layer BEM meshes with and without local mesh refinement. Following this, localization results with realistic data are shown. Again we used 0.33, 0.0042, 1.79, and 0.33 S/m for scalp, skull, CSF, and brain conductivities, respectively.

4.3.1. Effect of LMR ratio on 3-layer and 4-layer BEM head models

To compare the localization difference between 3-layer or 4-layer models of different mesh complexity, six different head models were generated using different LMR ratios. The results for the 4-layer BEM model with an LMR ratio of 1.6 were considered reference results, equivalent dipole source localization was performed for these potentials. For testing purposes, 24 dipoles of different eccentricities in three orthogonal directions inside the brain were simulated. Table 5 shows the properties of the meshes generated for this test. Mesh 4b, the finest mesh, was used as a reference for source localization.

A number of researchers have stated that including the highly conductive CSF layer in head models is important for accurate localization (Ramon et al., 2004; Akalin-Acar, 2005). Wendel et al. (2008) have shown how the CSF conductivity affects the scalp distribution of EEG, and Rullmann et al. (2009) investigated the effects on source localization of compartments (i.e., lesions) of varying conductivities. Source localization results are shown in Table 6. Adding the fourth (CSF) layer to the model gave an up to a 3-cm improvement in source localization. The effect of local mesh refinement

Table 5

Properties of the meshes used in the simulations.

Mesh name	Number of layers	Number of nodes	Number of faces	LMR ratio
Mesh 3	3	10,337	20,678	None
Mesh 3a	3	12,057	24,118	2
Mesh 3b	3	14,769	29,542	1.5
Mesh 4	4	13,775	27,550	None
Mesh 4a	4	18,499	36,998	2
Mesh 4b	4	20,789	41,578	1.6

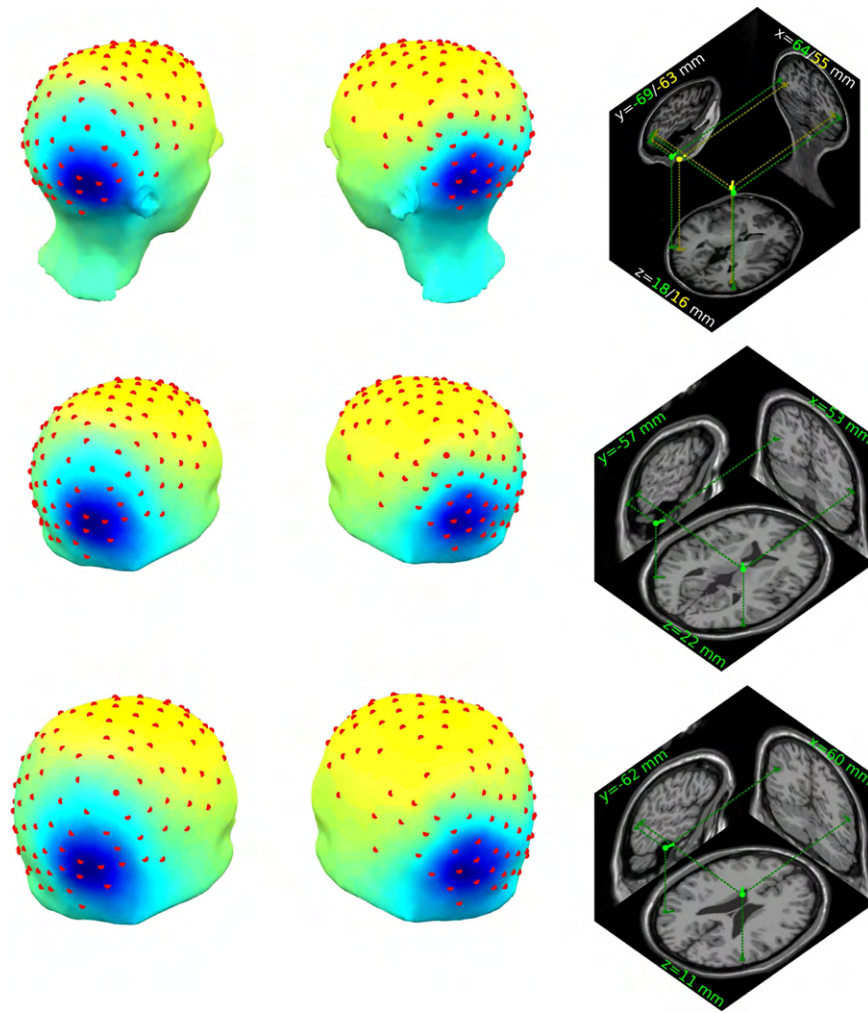


Fig. 11. Scalp projections (two left columns) and equivalent dipole source locations (right column) of two independent components extracted from a 140-electrode EEG recording by infomax ICA. Top row: Scalp maps and equivalent dipole positions computed using the individual subject MR-based BEM head models, (green dipoles) 4-layer and (yellow dipoles) 3-layer. Middle row: Scalp maps and equivalent dipole positions in the electrode position-warped standard 3-layer MNI head model. Bottom row: Scalp maps and equivalent dipole positions based on electrode positions warped to the standard 3-layer MNI head model. Slices shown are nearest to the (left posterior) equivalent dipole positions; their computed Talairach locations are shown (green/yellow lettering).

is also visible for the 4-layer meshes, for which mesh refinement improved localization accuracy by up to 1 cm.

4.3.2. Real EEG data example

In this section, source localization results for different head models are compared for one subject with an MR head image. EEG data were collected during a reaching task using 140 electrodes. Infomax Independent Component Analysis (ICA) (Bell and Sejnowski, 1995), developed for application to EEG data by Makeig et al. (1996) and Jung et al. (2001), was used to remove eye and muscle activity artifacts and also to identify and separate functionally independent cortical EEG processes. After ICA decomposition, single-dipole source localization was performed for two inde-

pendent component scalp maps that each highly resembled the projection of a single equivalent current dipole (likely representing the far-field potential projected by coherent field activity across a single cortical source patch).

Four realistic head models were generated using NFT from the subject MR head image: (a) a subject-specific realistic 4-layer BEM model; (b) a subject-specific realistic 3-layer BEM model; (c) an electrode position-warped MNI template model; (d) the standard MNI 3-layer BEM template model with electrode positions warped to the model head. In the 3-layer model, the CSF was included within the brain model compartment. The electrode position-warped head model was generated by warping the MNI template head model to the recorded scalp sensor locations using NFT, whereas in the MNI model, the recorded electrode locations were warped to the model MNI scalp surface using dipfit in EEGLAB.

Fig. 11 shows the component scalp maps and equivalent dipole source localization results. The electrode position-warped MNI model (middle row) is squeezed toward the back of the head and the equivalent dipole sources are localized closer to the surface compared to the sources localized using the standard MNI model (bottom row). In the 4-layer BEM model (top right, green), the equivalent dipoles are closer to the cortex because the highly conductive CSF tissue layer concentrates the flow of current within

Table 6
Localization error (LE) for 24 dipoles relative to Mesh 4b (in mm).

Mesh name	Mean LE	Minimum LE	Maximum LE
Mesh 3	17.1	7.1	23.7
Mesh 3a	16.1	3.9	26.2
Mesh 3b	16.9	4.1	29.3
Mesh 4	5.6	2.6	9.1
Mesh 4a	0.9	0.2	1.8
Mesh 4b	0.0	0.0	0.0

Table 7

The percentage residual variance (rv) of the scalp map versus the equivalent dipole map.

Head model	% rv (left component)	% rv (right component)
MR-based 4-layer	3.9	7.1
MR-based 3-layer	4.2	7.2
Position-warped MNI	2.9	7.5
Standard MNI	3.0	7.0

itself, reducing the diffusion produced by the current passing through the skull (Wolters et al., 2006; Wendel et al., 2008).

The residual variances of the scalp maps versus the equivalent dipole maps are close to each other across the different head models (Table 7), although the computed Talairach coordinates of the equivalent dipoles for the left component in the four head models (Fig. 11, right column) differed by up to more than 1 cm. More extensive comparisons for a large number of simulated equivalent dipole source positions (not shown here) demonstrate that differences in equivalent dipole locations between these head models vary with source location and orientation.

4.4. Known issues

A known problem with the segmentation module occurs when processing MR images with high inhomogeneity. Using fixed MRI intensity thresholds for scalp, skull and brain is insufficient if the image has inhomogeneity. The “Check Inhomogeneity” button in the segmentation user interface can be used to determine whether the current image needs correction. If this inhomogeneity check fails the function recommends performing inhomogeneity correction using a tool such as found in Freesurfer. The NFT user manual explains how to pre-process MR images.

5. Conclusion and discussion

Here we have introduced the Neuroelectromagnetic Forward Head Modeling Toolbox (NFT), a GUI-integrated collection of modules for defining and solving the EEG forward problem using realistic BEM or semi-realistic warped template head models. BEM head models may be generated from T1-weighted MR head images or by warping a template head mesh to recorded 3-D electrode locations.

Using the Boundary Element Method (BEM) allows easier mesh generation from available data compared with the Finite Element Method (FEM). While FEM potentially allows more accurate head models using more tissue types and allowing specification of tissue anisotropy, generating these models requires extra information such as direction anisotropy information gleaned from diffusion tensor (DT) images. For isotropic head models, BEM is at least as accurate as FEM and also provides better control over source dipole locations (Acar and Gençer, 1999).

The accuracy of the forward solution is also related to the size of the BEM mesh used to solve the forward problem. The distance between layers determine the maximum size of the elements. Typical four layer meshes generated by NFT have about 19,000 nodes. The most memory intensive computation in NFT is the generation of BEM matrices done by the METU-BEM toolkit. The memory used for matrix computations is slightly larger than the total size of the BEM matrices. For subject-specific realistic models generated by the toolbox, this will be approximately 4.8 GB of memory using IPA and 3 GB not using IPA. A 3-layer mesh without IPA requires only 1.6 GB for generating the matrices.

While the BEM matrix generation is resource intensive, it is within the capabilities of modern workstations. Once the transfer matrices are generated, individual forward problem solutions

take much less memory and computational resources. It may be possible to reduce the memory requirements further by parallelization (Ataseven et al., 2008). On-disk size of the matrices can also be reduced by using data compression techniques. These features are planned for future releases. Other future plans include improving image segmentation to use multi-modal MR images which will allow increased accuracy of CSF segmentation. We also plan to add software for performing inverse source imaging using a high resolution cortical surface-derived source space. Adding other forward problem solvers including FEM and analytical concentric spheres is also being considered.

The NFT includes an interface to EEGLAB, and EEGLAB functions and data structures are compatible with NFT structures. The toolbox released under the GPL(v2) license may be downloaded from <http://sccn.ucsd.edu/nft> or via the EEGLAB web site (<http://sccn.ucsd.edu/eeglab/>)

Acknowledgments

The authors gratefully acknowledge the assistance of Dr. Jeng-Ren Duann and Dr. Ruey-Song Huang in acquiring the MR images and Dr. Yijun Wang in processing the EEG data. The authors would also like to thank Dr. Nevzat Gençer, for his vision and commitment to realistic head modeling. The BEM solver and parts of the segmentation and mesh generation effort were created under his supervision. This work was supported by gifts from the Swartz Foundation (Old Field, NY) and by NIH/NINDS (NS047293-04).

References

- Acar CE, Gençer NG. Forward problem solution of ESI using FEM and BEM with quadratic isoparametric elements. In: Proceedings of IEEE EMBS conference; September, 1999.
- Akalin Acar Z. Electro-magnetic source imaging using realistic head models. Ph.D. Thesis. University of Middle East Technical University, Ankara; 2005.
- Akalin-Acar Z, Gençer NG. An advanced boundary element method (BEM) implementation for the forward problem of electromagnetic source imaging. *Phys Med Biol* 2004;49:5011–28 [available at <http://www.eee.metu.edu.tr/metufp/>].
- Akalin Acar Z, Makeig S. Neuroelectromagnetic forward modeling toolbox. In: Proceedings of IEEE EMBC; 2008.
- Ataseven Y, Akalin-Acar Z, Acar CE, Gençer NG. Parallel implementation of the accelerated BEM approach for EMSI of the human brain. *Med Biol Eng Comput* 2008;46:671–9.
- Baumann S, Wozny D, Kelly S, Meno F. The electrical conductivity of human cerebrospinal fluid at body temperature. *IEEE Trans Biomed Eng* 1997;3:220–3.
- Bell AJ, Sejnowski TJ. An information-maximization approach to blind separation and blind deconvolution. *Neural Comput* 1995;7:1129–59.
- Bookstein F. Linear methods for nonlinear maps: procrustes fits, thin-plate splines, and the biometric analysis of shape variability. In: *Brain warping*. New York: Academic Press; 1999. p. 157–81.
- Chu V, Hamarneh G. Matitk: extending MATLAB with ITK. *The Insight Journal*; 2005 [available at <http://www.sfu.ca/vvchu/matitk.html>].
- Cohen D, Cuffin NB, Yunokuchi K, Maniewski R, Purcell C, Cosgrove RG, et al. MEG versus EEG localization test using implanted sources in the human brain. *Ann Neurol* 1990;28(6):811–7.
- Crouzeix A, Yvert B, Bertrand O, Pernier J. An evaluation of dipole reconstruction accuracy with spherical and realistic head models in MEG. *Clin Neurophysiol* 1999;110:2176–88.
- Cuffin NB. EEG localization accuracy improvements using realistically shaped head models. *IEEE Trans Biomed Eng* 1996;44(3):299–303.
- Darvas F, Ermer J, Mosher J, Leahy R. Generic head models for atlas-based EEG source analysis. *Hum Brain Map* 2006;27:129–43.
- Delorme A, Makeig S. Eeglab: an open source toolbox for analysis of single-trial EEG dynamics including independent component analysis. *J Neurosci M* 2004;134:9–21 [available at <http://www.sccn.ucsd.edu/eeglab/>].
- Drechsler F, Wolters C, Dierkes T, Si H, Grasedyck L. A full subtraction approach for finite element method based source analysis using constrained delaunay tetrahedralisation. *NeuroImage* 2009;46(3):1055–65.
- Garland M, Shaffer E. A multiphase approach to efficient surface simplification. *Visualization*; 2002:117–24 [available at <http://mgarland.org/software/qslim.html>].
- Geddes LA, Baker LE. The specific resistance of biological materials—a compendium of data for the biomedical engineer and physiologist. *Med Biol Eng* 1967;5:271–93.
- Gençer NG, Acar CE. Sensitivity of EEG and MEG measurements to tissue conductivity. *Phys Med Biol* 2004;49:701–17.

- Gençer NG, Akalin-Acar Z. Use of the isolated problem approach for multi-compartment BEM models of electro-magnetic source imaging. *Phys Med Biol* 2005;50:3007–22.
- Gençer NG, Tanzer IO. Forward problem solution of electromagnetic source imaging using a new BEM formulation with high-order elements. *Phys Med Biol* 1999;44:2275–87.
- Guziec A, Taubin G, Lazarus F, Horn B. Cutting and stitching: converting sets of polygons to manifold surfaces. *IEEE Trans Visual Comput Graph* 2001;7(2):136–51.
- Heckbert PS, Garland M. Optimal triangulation and quadric-based surface simplification. *Comput Geomet* 1999;14:49–65.
- Heinonen T, Dastidar P, Kauppinen P, Malmivuo J, Eskola H. Semi-automatic tool for segmentation and volumetric analysis of medical images. *Med Biol Eng Comput* 1998;36:291–6.
- Henderson CJ, Butler SR. The localization of equivalent dipoles of EEG sources by the application of electrical field theory. *Neurophysiology* 1975;39:117–30.
- Ibanez L, Schroeder W, Ng L, Cates L. The ITK software guide, second edition, New York: Kitware, Inc; 2005 [available online at <http://www.itk.org/>].
- Jung T, Makeig S, Mckeown MJ, Bell AJ, Lee T, Sejnowski TJ. Imaging brain dynamics using independent component analysis. *Proc IEEE* 2001;89:1107–22.
- Kavanagh RN, Darcey TM, Lehmann D, Fender DH. Evaluation of method for three-dimensional localization of electrical sources in the human brain. *IEEE Trans Biomed Eng* 1978;25:421–9.
- Kruggel F, Lohmann G. Brian a toolkit for the analysis of multimodal brain datasets. In: *Proceedings of the computer aided radiology*; 1996. p. 323–8.
- Lynn MS, Timlake WP. The use of multiple deflations in the numerical solution of singular systems of equations, with applications to potential theory. *SIAM J Numer Anal* 1968;5:303–22.
- Makeig S, Bell AJ, Jung T, Sejnowski T. Independent component analysis of electroencephalographic data. In: *Advances in neural information processing systems*, vol. 8. Cambridge: MIT Press; 1996. p. 145–51.
- Meijs JWH, Weier O, Peters MJ. On the numerical accuracy of the boundary element method. *IEEE Trans Biomed Eng* 1989;36:1038–49.
- Nobuyuki O. A threshold selection method from gray-level histograms. *IEEE Trans Syst Man Cybern* 1979;SMC-9(1):62–6.
- Poston T, Wong T, Heng P. Multiresolution isosurface extraction with adaptive skeleton climbing. In: *Proceedings of eurographics*, vol. 17; 1998 [available at <http://www.cse.cuhk.edu.hk/ttwong/papers/asc/asc.html>].
- Ramon C, Schimpf P, Haueisen J, Holmes M, Ishimaru A. Role of soft bone, CSF and gray matter in EEG simulations. *Brain Topography* 2004;16(4):245–8.
- Riviere D, Regis J, Cointepas Y, Papadopoulos-Orfanos D, Ochiai T, Cachia A et al. A freely available anatomist/brainvisa package for structural morphometry of the cortical sulci. In: *Proceedings 9th HBM CD-rom neuroimage*, vol. 19; 2003 [available at <http://brainvisa.info/>].
- Roth BJ, Balish M, Gorbach A, Sato S. How well does a three-sphere model predict positions of dipoles in a realistically shaped head? *Electroenceph Clin Neurophysiol* 1993;87:175–84.
- Rullmann M, Anwander A, Dannhauer M, Warfield S, Duffy FH, Wolters C. EEG source analysis of epileptiform activity using a 1 mm anisotropic hexahedra finite element head model. *NeuroImage* 2009;44(2):399–410.
- Shattuck DW, Leahy RM. BrainSuite: an automated cortical surface identification tool. *Med Image Anal* 2002;6:129–42 [available at <http://brainsuite.usc.edu/>].
- Smith S. Fast robust automated brain extraction. *Hum Brain Map* 2002;17:143–55.
- Talairach J, Tournoux P. *Co-planar stereotaxic atlas of the human brain*. New York: Thieme Medical Publishers; 1998.
- Taubin G. A signal processing approach to fair surface design. In: *Proceedings of Siggraph*; 1995. p. 351–8.
- Weinberg H, Brickett P, Coolsma F, Baff M. Magnetic localization of intracranial dipoles: simulation with a physical model. *Electroenceph Clin Neurophysiol* 1986;64:159–70.
- Wendel K, Narra N, Hannula M, Kauppinen P, Malmivuo J. The influence of CSF on EEG sensitivity distributions of multilayered head models. *IEEE Trans Biomed Eng* 2008;55(4):1454–6.
- Wolters C, Anwander A, Tricoche X, Weinstein D, Koch M, MacLeod R. Influence of tissue conductivity anisotropy on EEG/MEG field and return current computation in a realistic head model: a simulation and visualization study using high-resolution finite element modelling. *NeuroImage* 2006;30(3):813–26.
- Wolters C, Köstler H, Möller C, Härtlein J, Grasedyck L, Hackbusch W. Numerical mathematics of the subtraction method for the modeling of a current dipole in EEG source reconstruction using finite element head models. *SIAM J Sci Comput* 2007;30(1):24–45.
- Wolters CH, Kuhn M, Anwander A, Reitzinger S. A parallel algebraic multigrid solver for finite element method based source localization in the human brain. *Comput Visual Sci* 2002;5:165–77.
- Zhang Z, Jewett D. Insidious errors in dipole localization parameters at a single time-point due to model misspecification of number of shells. *Electroenceph Clin Neurophysiol* 1993;88:1–11.
- Zhang Z, Jewett D, Goodwill G. Insidious errors in dipole parameters due to shell model misspecification using multiple time points. *Brain Topography* 1994;6:283–98.